LN

Multiband Phase Space Operator for Narrow Bandgap Semiconductor Devices

1st Lukas Schulz
High Frequency Institute
TU Dortmund
Dortmund, Germany
lukas.schulz@tu-dortmund.de

2nd Dirk Schulz
High Frequency Institute
TU Dortmund
Dortmund, Germany
dirk2.schulz@tu-dortmund.de

***Abstract*—The analysis of the charge carrier transport within modern device concepts of nanoelectronics and nanophotonics as well as THz technology requires the inclusion of multiband Hamiltonians. These can then be used to consider not only intraband transitions but also interband transitions as well as effects based on the existence and interaction of light and heavy holes. For this purpose appropriate multiband Hamiltonians must be applied for a suitable numerical analysis. On the basis of the quantum Liouville equation, a formalism is derived how multiband Hamiltonians can be integrated into advanced and recently developed Wigner transport based algorithms utilizing a phase space operator and which multiband models are appropriate. The presented formalism is demonstrated by its application onto resonant tunnel diodes that take advantage of interband effects within narrow band gap semiconductor devices.**

***Index Terms*—Interband tunneling, multiband Hamiltonians, phase space operator, Wigner equation.**

I. Introduction

The quantum mechanical description of nanoelectronic devices in terms of a phase space formulation provided by the Wigner formalism is of considerable interest as this formalism offers the possibility to analyze transient effects and to incorporate interaction mechanisms effectively. So far, Wigner based formalisms are predominantly based on single band approximations considering the conduction band but are lacking of the inclusion of multiband models. Typically, existing formalisms are applied onto large bandgap double barrier resonant tunneling diodes [1]–[3] and field effect transistors [4]–[6], so that intraband dynamics essentially affect the device performance. However, when the bandgap shrinks and band-coupling effects shall be considered, the corresponding interband kinetics must be adequately included.

A recently proposed Wigner based formalism is extended, which is based on a phase space operator [7] considering nonlocal quantum effects and on the complex absorbing potential (CAP) formalism [8] in order to adequately account for the finiteness of the computational domain.

Two distinct multiband approaches are suitable for the application within the Wigner formalism, namely the two band Kane-model [9] as well as the multiband-envelope function (MEF)-model [10], [11]. The latter model leads to a similar formulation as in the Luttinger-Kohn-model, however, in comparison the interband kinetics are not neglected. The MEF-model is preferable due to the direct physical interpretation of the electron and hole wave functions [12]. In addition, the interband coupling is only present in the case of a non constant external potential. This fact leads to a simplification of the formulation of boundary conditions as intermixing states are avoided at the boundaries. Because of the enumerated reasons, the MEF-model is particularly distinctive and, therefore, is applied onto the Wigner equation.

The authors gratefully acknowledge the financial support by the German Research Funding Association Deutsche Forschungsgemeinschaft under grant SCHU-2016/8-1.

II. MEF-Wigner Transport Equation

To demonstrate the approach, the two band Schrödinger equation within the MEF framework [12] is chosen and given by

$$\imath\hbar\frac{\partial}{\partial t}\mathbf{\Psi}(z,t)=\mathcal{H}\mathbf{\Psi}(z,t)=\begin{bmatrix} H_{\mathrm{c}}(z) & H_{\mathrm{i}}(z) \\ H_{\mathrm{i}}(z) & H_{\mathrm{v}}(z)\end{bmatrix}\mathbf{\Psi}(z,t), \quad (1)$$

where the vector $\mathbf{\Psi}=(\Psi_{\mathrm{c}}(z),\Psi_{\mathrm{v}}(z))^T$ contains the wavefunctions for the conduction band Ψ_{c} as well as the valence band Ψ_{v}. The diagonal terms of the Hamiltonian $\mathcal{H}$ describe the intraband dynamics, whereas the off-diagonal elements account for the interband dynamics. The Hamiltonian $\mathcal{H}$ is defined according to

$$\begin{aligned} H_{\mathrm{c,v}}(z)&=-\frac{\hbar^2}{2m_{\mathrm{c,v}}}\frac{\partial^2}{\partial z^2}+E_{\mathrm{c,v}}+V(z)\\ H_{\mathrm{i}}(z)&=-\frac{\hbar^2 P}{m_0 E_g}\frac{\partial}{\partial z}V(z), \end{aligned} \quad (2)$$

where m_{c} and m_{v} are the effective masses of the conduction band and the valence band, respectively, and m_0 is the free electron mass. $V(z)$ includes the external applied biases, the self-consistent Hartree-Fock potential as well as the bandgap discontinuities due to heterostructures [12]. The parameter P is related to Kane's matrix momentum element and $E_g = E_{\mathrm{c}} - E_{\mathrm{v}}$ is the bandgap determined by the conduction band edge energy E_{c} and valence band edge energy E_{v}.

The elements of the real space statistical density matrix ρ_{ij} with $i,j=\mathrm{c},\mathrm{v}$ are defined as

$$\rho_{ij}=\Psi_i\left(\chi+\frac{1}{2}\xi,t\right)\Psi_j^{\dagger}\left(\chi-\frac{1}{2}\xi,t\right) \quad (3)$$

© 2020 The Japan Society of Applied Physics

and after the application of the Wigner-Weyl transform the following multiband Wigner functions f_{ij} result:

$$f_{ij}(\chi,k,t)=\int \mathrm{d}\xi\ \exp\left(-\imath k\xi\right)\cdot\rho_{ij}\left(\chi+\frac{1}{2}\xi,\chi-\frac{1}{2}\xi,t\right). \tag{4}$$

Finally, the application of the Wigner-Weyl transform onto the Liouville von Neumann equation leads to a system of coupled Wigner equations

$$\begin{aligned}
\frac{\partial}{\partial t}f_{\mathrm{cc}}&=+\mathcal{A}\frac{\partial}{\partial\chi}f_{\mathrm{cc}}+\Theta[\hat{V}]f_{\mathrm{cc}}+\Theta[\hat{V}^{-}]f_{\mathrm{cv}}-\Theta[\hat{V}^{+}]f_{\mathrm{vc}}\\
\frac{\partial}{\partial t}f_{\mathrm{cv}}&=+\left[\mathcal{D}\frac{\partial^2}{\partial\chi^2}+\mathcal{G}\right]f_{\mathrm{cv}}+\Theta[\hat{V}]f_{\mathrm{cv}}+\\
&\qquad\qquad\Theta[\hat{V}^{-}]f_{\mathrm{cc}}-\Theta[\hat{V}^{+}]f_{\mathrm{vv}},\\
\frac{\partial}{\partial t}f_{\mathrm{vc}}&=-\left[\mathcal{D}\frac{\partial^2}{\partial\chi^2}+\mathcal{G}\right]f_{\mathrm{vc}}+\Theta[\hat{V}]f_{\mathrm{vc}}+\\
&\qquad\qquad\Theta[\hat{V}^{-}]f_{\mathrm{vv}}-\Theta[\hat{V}^{+}]f_{\mathrm{cc}}\\
\frac{\partial}{\partial t}f_{\mathrm{vv}}&=-\mathcal{A}\frac{\partial}{\partial\chi}f_{\mathrm{vv}}+\Theta[\hat{V}]f_{\mathrm{vv}}+\Theta[\hat{V}^{-}]f_{\mathrm{vc}}-\Theta[\hat{V}^{+}]f_{\mathrm{cv}}
\end{aligned} \tag{5}$$

where the occuring operators are defined as follows:

$$\mathcal{A}=-\frac{\hbar k}{m},\quad \mathcal{D}=-\frac{\hbar}{4\imath m},\quad \mathcal{G}=\frac{1}{\imath\hbar}\left\{\frac{\hbar^2k^2}{m}+E_g\right\}, \tag{6}$$

$$\Theta[\hat{V}]f_{ij}=\frac{1}{\imath\hbar}\int\frac{\mathrm{d}k'}{2\pi}\hat{V}(\chi,k-k')f_{ij}(\chi,k',t) \tag{7}$$

and

$$\Theta[\hat{V}^{\pm}]f_{ij}=\frac{\hbar P}{\imath m_0E_g}\int\frac{\mathrm{d}k'}{2\pi}\ \hat{V}^{\pm}(\chi,k-k')f_{ij}(\chi,k',t). \tag{8}$$

Additionally, for the demonstration of the multiband formalism, the effective masses within the conduction band are assumed to be equal with $m=m_{\mathrm{c}}=-m_{\mathrm{v}}$, so that a comparison with results obtained by existing multiband approaches could be possible, i.e. [11]. However, the extension is straightforward and does not affect the multiband formalism as well as the discretization due to the phase space operator presented here. The terms including the potential distributions are given by

$$\begin{aligned}
\hat{V}(\chi,k)&=\int\mathrm{d}\xi\ \exp\left(-\imath k\xi\right)\\
&\times\left\{V\left(\chi+\frac{1}{2}\xi\right)-V\left(\chi-\frac{1}{2}\xi\right)-\imath W(\xi)\right\},
\end{aligned} \tag{9}$$

where the CAP has been introduced by an addend $\imath W(\xi)$. The terms related to the interband dynamics are defined by

$$\hat{V}^{\pm}(\chi,k)=\int\mathrm{d}\xi\ \exp\left(-\imath k\xi\right)\mathcal{E}\left(\chi\pm\frac{1}{2}\xi\right) \tag{10}$$

introducing the electrical field $\mathcal{E}(z)=-\frac{\mathrm{d}}{\mathrm{d}z}V(z)$. As can be observed from these coupled Wigner equations, the standard single band Wigner equation for the conduction band arises from (5), when no external potentials are present or the Kane's matrix momentum is set to zero.

A. Numerical Discretization

For the numerical solution of the system of coupled Wigner equations (5), the formalism proposed in [7], [13] for the single band case is extended towards the multiband case. The momentum variable is discretized utilizing a standard finite difference scheme leading to a semi-discrete Wigner equation, which then is solved along with the phase space operator as in [13]. Due to the discretization utilizing N_k discretization points, only a finite range of momentum related values k within the interval $[-k_{\max},k_{\max}]$ can be taken into account. Conceptually, the discretization of (5) with regard to the momentum variable k results in a system of coupled partial differential equations, which can be written as

$$\begin{aligned}
\frac{\partial}{\partial t}\boldsymbol{f}_{\mathrm{cc}}&=+\boldsymbol{A}\frac{\partial}{\partial\chi}\boldsymbol{f}_{\mathrm{cc}}+\boldsymbol{B}(\chi)\boldsymbol{f}_{\mathrm{cc}}+\boldsymbol{B}^{-}(\chi)\boldsymbol{f}_{\mathrm{cv}}-\boldsymbol{B}^{+}(\chi)\boldsymbol{f}_{\mathrm{vc}}\\
\frac{\partial}{\partial t}\boldsymbol{f}_{\mathrm{cv}}&=+\left\{\boldsymbol{D}\frac{\partial^2}{\partial\chi^2}+\boldsymbol{G}\right\}\boldsymbol{f}_{\mathrm{cv}}+\boldsymbol{B}(\chi)\boldsymbol{f}_{\mathrm{cv}}+\\
&\qquad\qquad\boldsymbol{B}^{-}(\chi)\boldsymbol{f}_{\mathrm{cc}}-\boldsymbol{B}^{+}(\chi)\boldsymbol{f}_{\mathrm{vv}}\\
\frac{\partial}{\partial t}\boldsymbol{f}_{\mathrm{vc}}&=-\left\{\boldsymbol{D}\frac{\partial^2}{\partial\chi^2}+\boldsymbol{G}\right\}\boldsymbol{f}_{\mathrm{vc}}+\boldsymbol{B}(\chi)\boldsymbol{f}_{\mathrm{vc}}+\\
&\qquad\qquad\boldsymbol{B}^{-}(\chi)\boldsymbol{f}_{\mathrm{vv}}-\boldsymbol{B}^{+}(\chi)\boldsymbol{f}_{\mathrm{cc}}\\
\frac{\partial}{\partial t}\boldsymbol{f}_{\mathrm{vv}}&=-\boldsymbol{A}\frac{\partial}{\partial\chi}\boldsymbol{f}_{\mathrm{vv}}+\boldsymbol{B}(\chi)\boldsymbol{f}_{\mathrm{vv}}+\boldsymbol{B}^{-}(\chi)\boldsymbol{f}_{\mathrm{vc}}-\boldsymbol{B}^{+}(\chi)\boldsymbol{f}_{\mathrm{cv}}
\end{aligned} \tag{11}$$

Due to the discretization, the diffusion process related operators $\mathcal{A}\rightarrow\boldsymbol{A},\mathcal{D}\rightarrow\boldsymbol{D}$ and the intraband dynamics related drift operators $\mathcal{G}\rightarrow\boldsymbol{G},\Theta[V]\rightarrow\boldsymbol{B}$ as well as the interband dynamics related drift operator $\Theta[V^{\pm}]\rightarrow\boldsymbol{B}^{\pm}$ are introduced. The elements of the corresponding matrix representation (11) are indicated by the subscripts $j,j'\in 1,\ldots,N_k$ and given by

$$\begin{aligned}
\boldsymbol{A}_{j,j'}&=\frac{-\hbar k_j}{m}\delta_{j,j'} & \boldsymbol{D}_{j,j'}&=\frac{-\hbar}{4\imath m}\delta_{j,j'}\\
\boldsymbol{G}_{j,j'}&=\left\{\frac{\hbar^2k^2}{m}+E_g\right\}\frac{\delta_{j,j'}}{\imath\hbar} & \boldsymbol{B}_{j,j'}&=\frac{\Delta k}{2\pi}\frac{\hat{V}(\chi,k_j-k'_j)}{\imath\hbar}\\
&& \boldsymbol{B}^{\pm}_{j,j'}&=\frac{\hbar P}{\imath m_0E_g}\frac{\Delta k}{2\pi}\hat{V}^{\pm}(\chi,k_j-k'_j)
\end{aligned} \tag{12}$$

with $\delta_{j,j'}$ being the Kronecker-delta. The approximation of the integral kernels, as apparent in the drift related matrices $\boldsymbol{G}$, $\boldsymbol{B}$ and $\boldsymbol{B}^{\pm}$, is carried out applying a standard midpoint rule leading to the relations

$$\begin{aligned}
\hat{V}(\chi,k_j-k'_j)&=\sum_{i=1}^{N_k}\Delta\xi\exp\left(-\imath(k_j-k'_j)\xi_i\right)\cdot\\
&\qquad\left\{V\left(\chi+\frac{\xi_i}{2}\right)-V\left(\chi-\frac{\xi_i}{2}\right)-\imath W(\xi_i)\right\}\\
\hat{V}^{\pm}(\chi,k_j-k'_j)&=\sum_{i=1}^{N_k}\Delta\xi\exp\left(-\imath(k_j-k'_j)\xi_i\right)\cdot\mathcal{E}\left(\chi\pm\frac{\xi_i}{2}\right)
\end{aligned} \tag{13}$$

The system of coupled discretized Wigner equations is reformulated in order to derive a phase space operator addressing the spatial approximation with regard to the variable χ and

following the concept as described in [13]. Furthermore, a supervector $\boldsymbol{f} = (\boldsymbol{f}_{\mathrm{cc}}, \boldsymbol{f}_{\mathrm{cv}}, \boldsymbol{f}_{\mathrm{vc}}, \boldsymbol{f}_{\mathrm{vv}})^T$ is introduced containing all the discretized Wigner functions (4). Along with these abbreviations, the coupled Wigner equations (11) can be rewritten as

$$\left[\boldsymbol{D_2}\frac{\mathrm{d}^2}{\mathrm{d}\chi^2} + \boldsymbol{D_1}\frac{\mathrm{d}}{\mathrm{d}\chi} + \boldsymbol{D_0}(\chi)\right]\boldsymbol{f}(\chi) = 0, \tag{14}$$

which is the standard form for the derivation of the phase space operators containing a derivative up to the 2nd order in the χ-direction [13]. The matrices $[\boldsymbol{D_2}], [\boldsymbol{D_1}], [\boldsymbol{D_0}]$ of the order $4N_k \times 4N_k$ are given by

$$\begin{aligned}
\boldsymbol{D_2} &= \mathrm{diag}\,(\boldsymbol{0}, \boldsymbol{D}, -\boldsymbol{D}, \boldsymbol{0}) \\
\boldsymbol{D_1} &= \mathrm{diag}\,(\boldsymbol{A}, \boldsymbol{0}, \boldsymbol{0}, -\boldsymbol{A}) \\
\boldsymbol{D_0}(\chi) &= \begin{bmatrix} \boldsymbol{B}(\chi) & \boldsymbol{B}^-(\chi) & -\boldsymbol{B}^+(\chi) & \boldsymbol{0} \\ \boldsymbol{B}^-(\chi) & \boldsymbol{B}(\chi) + \boldsymbol{G} & \boldsymbol{0} & -\boldsymbol{B}^+(\chi) \\ -\boldsymbol{B}^+ & \boldsymbol{0} & \boldsymbol{B}(\boldsymbol{\chi}) - \boldsymbol{G} & \boldsymbol{B}^-(\chi) \\ \boldsymbol{0} & -\boldsymbol{B}^+(\chi) & \boldsymbol{B}^-(\chi) & \boldsymbol{B}(\chi) \end{bmatrix}
\end{aligned} \tag{15}$$

with $\boldsymbol{0}$ being a $N_k \times N_k$ zero-valued matrix. As can be observed, only the matrix $\boldsymbol{D_0}$ contains non zero-valued off-(block-)diagonal elements including the interband coupling effects. Following the procedure as described in detail in [13], the discretized Wigner functions $\boldsymbol{f}_{ij}$ are obtained.

B. Inflow Boundary Conditions for Quantum Transport

Similar to the conventional single band case [1]–[3], a quantum statistical distribution function has to be defined at the boundaries. The injection of electrons is then related to the sign of the corresponding momentum k. The inflow of electrons is provided by the distribution function $f^e_{l,r}$ for the left contact considering positive values and for the right contact with negative values given by

$$f_{\mathrm{cc}}(\chi_{1,N_\chi}, k \gtrless 0, t) = f^e_{l,r}(k \gtrless 0). \tag{16}$$

For the hole transport, a relationship must be chosen in a way so that the holes are injected where the electrons are flowing out [14] leading to

$$f_{\mathrm{vv}}(\chi_{1,N_\chi}, k \gtrless 0, t) = f^h_{l,r}(k \gtrless 0) \tag{17}$$

with $f^h_{l,r}$ being the hole distribution function at the left and right contact. Obviously, the components $\boldsymbol{f}_{\mathrm{cv}}$ and $\boldsymbol{f}_{\mathrm{vc}}$ of the discretized Wigner function can be assumed to be zero-valued functions at the boundaries of the computational domain. In addition, von-Neumann boundary conditions are provided, namely

$$\frac{\mathrm{d}}{\mathrm{d}\chi} f_{\mathrm{cv}} = \frac{\mathrm{d}}{\mathrm{d}\chi} f_{\mathrm{vc}} = 0. \tag{18}$$

In a similar manner as for the single band case described in [13], the boundary conditions are incorporated into the system matrix.

	contact	spacer	barrier	well	barrier	spacer	contact
L in nm	30	15	3	5	3	15	30
V in eV	0	0	0.11	0.51	0.11	0	0

TABLE I: Parameters of the resonant interband tunneling diode.

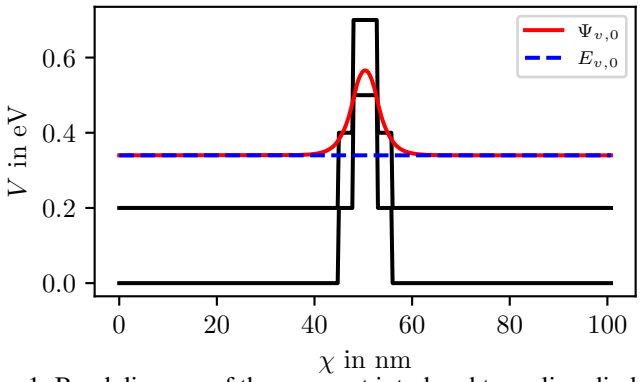

Fig. 1: Band diagram of the resonant interband tunneling diode along with the wavefuntion $\Psi_{v,0}$ (with $E_{v,0}$) of the bounded state within the valence band is depicted.

III. Numerical Evaluation

To demonstrate the capability of the proposed formalism, a resonant structure is analyzed, in which interband tunneling effects are assumed to be prominent leading to a negative differential resistance. Here, a similar structural and material parameters are adopted from [11]. The relevant structural parameters of the resonant interband tunneling diode are provided in Table I and the band diagram is depicted in Fig. 1. The bounded valence band state $\Psi_{v,0}$ located at approximately $E_{v,0} = 0.34$eV is depicted, too, as the results obtained later on are discussed with regard to the bounded valence band state. This bounded state serves as the resonant state and its value $E_{v,0}$ is obtained by solving the Schrödinger equation. For the discretization of the computational domain, a step width size $\Delta\chi = 0.25$nm has been chosen. The momentum grid is discretized along with $N_k = 100$ discretization points within the interval $[-1.5\mathrm{nm}^{-1}, 1.5\mathrm{nm}^{-1}]$. The band gap is assumed to be $E_g = 0.2$eV and the momentum matrix element is set to $P = 5\mathrm{nm}^{-1}$. The effective mass is set to a value of $m = 0.027m_0$ and the doping concentration at the contacts is $1 \cdot 10^{24}\mathrm{m}^{-3}$.

The current-voltage characteristic for the device is depicted in Fig. 2 presuming a linear voltage drop in between the left and right contact regions. The bias sweep within 0V and 0.55V is discretized with 56 points and the current density obtained for each discrete bias point is obtained by summing up both current densities stemming from the conduction as well as the valence band [13]. As expected, the negative differential resistance behavior can be observed and coincides with the result given in [12]. In addition, when analyzing the location the current peak at approximately $U_{\mathrm{peak}} \approx 0.13$V, a fairly good agreement with the determined eigenenergy $E_{v,0}$ of the resonant state can be established. This resonant state is about 0.14eV above the conduction band energy, additionally justifying the qualitative behavior of the current

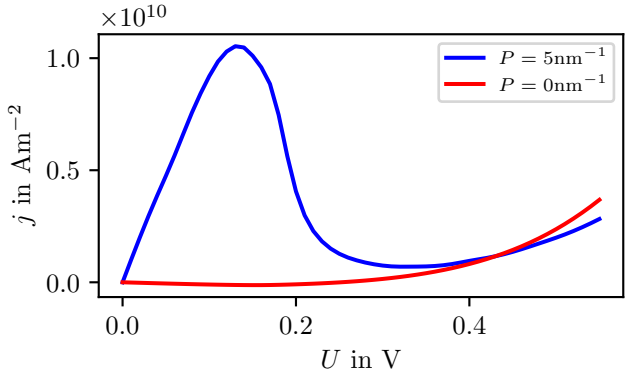

Fig. 2: Current-voltage characteristic for the resonant interband tunneling diode.

density. Furthermore, when the momentum matrix element P is zero valued, no negative differential resistance can be observed from Fig. 2 as expected. Further on, the carrier densities for the valence band n_v, the conduction band n_c and the corresponding sum $n = n_c + n_v$ are shown in Fig. 3 for the peak voltage at about $U_{\text{peak}} = 0.13\text{V}$ as well as for the valley voltage at about $U_{\text{valley}} = 0.35\text{V}$, respectively. These densities are determined by taking the zeroth order moment of the corresponding Wigner function. The carrier density for the peak voltage case U_{peak} exhibits large values within the well region due to the strong interaction with the resonant state, which assists the tunneling process. However, when the carrier density for the valley voltage U_{valley} is considered, the resonant state does not contribute to the transport process leading to an extremely small density within the well regions.

IV. Conclusion

The proposed formalism forms the basis for further device oriented analysis, for which different band edge discontinuities, different effective masses e. g. related to the Luttinger-Kohn parameters, multiband models including strain effects as well as different momentum matrix elements and their spatial dependence can be considered revealing the full potential of the Wigner formalism.

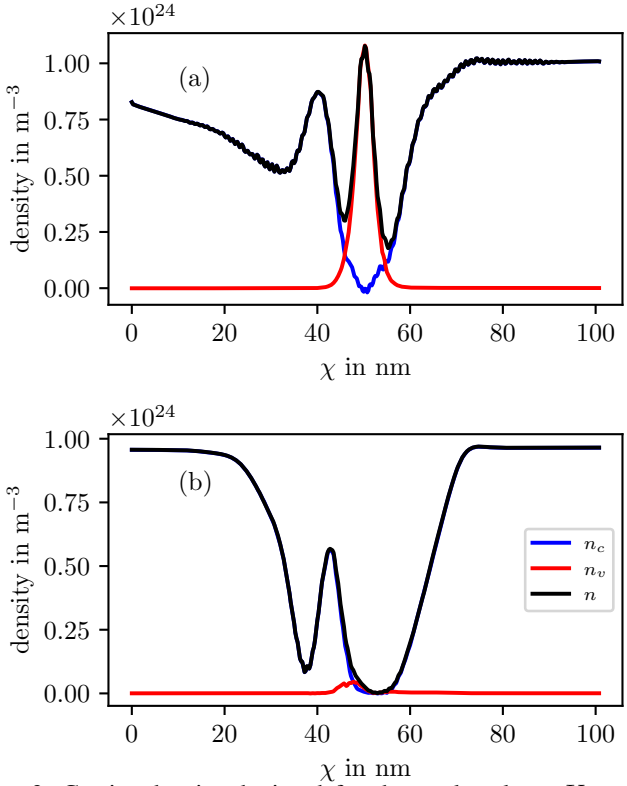

Fig. 3: Carrier density depicted for the peak voltage $U_{\text{peak}} = 0.13\text{V}$ (a) and $U_{\text{valley}} = 0.35\text{V}$ (b).

References

[1] W. R. Frensley, "Wigner-function model of a resonant-tunneling semiconductor device," *Phys. Rev. B*, vol. 36, pp. 1570–1580, 3 Jul. 1987.

[2] ——, "Boundary conditions for open quantum systems driven far from equilibrium," *Rev. Mod. Phys.*, vol. 62, pp. 745–791, 3 Jul. 1990.

[3] H. Tsuchiya, M. Ogawa, and T. Miyoshi, "Simulation of quantum transport in quantum devices with spatially varying effective mass," vol. 38, no. 6, pp. 1246–1252, Jun. 1991.

[4] D. Querlioz, J. Saint-Martin, V. Do, A. Bournel, and P. Dollfus, "A study of quantum transport in end-of-roadmap dg-mosfets using a fully self-consistent wigner monte carlo approach," vol. 5, no. 6, pp. 737–744, Nov. 2006.

[5] H. Kosina, "Wigner function approach to nano device simulation," *Int. J. Comput. Eng. Sci.*, vol. 2, no. 3-4, pp. 100–118, 2006.

[6] H. Jiang and W. Cai, "Effect of boundary treatments on quantum transport current in the green's function and wigner distribution methods for a nano-scale dg-mosfet," *J. Comput. Phys.*, vol. 229, no. 12, pp. 4461–4475, 2010.

[7] D. Schulz and A. Mahmood, "Approximation of a phase space operator for the numerical solution of the wigner equation," vol. 52, no. 2, pp. 1–9, 2016.

[8] L. Schulz and D. Schulz, "Complex absorbing potential formalism accounting for open boundary conditions within the wigner transport equation," vol. 18, pp. 830–838, 2019.

[9] G. Borgioli, G. Frosali, and P. F. Zweifel, "Wigner approach to the two-band kane model for a tunneling diode," *Transp. Theory Stat. Phys.*, vol. 32, no. 3-4, pp. 347–366, 2003.

[10] O. Morandi, "Multiband wigner-function formalism applied to the zener band transition in a semiconductor," *Phys. Rev. B*, vol. 80, p. 024 301, 2 Jul. 2009.

[11] G. Frosali and O. Morandi, "A quantum kinetic approach for modeling a two-band resonant tunneling diode," *Transp. Theory Stat. Phys.*, vol. 36, no. 1-3, pp. 159–177, 2007.

[12] O. Morandi and M. Modugno, "Multiband envelope function model for quantum transport in a tunneling diode," *Phys. Rev. B*, vol. 71, no. 23, Jun. 2005.

[13] L. Schulz and D. Schulz, "Formulation of a phase space operator accounting for the spatial variation of the effective mass within the wigner equation," *J. Comput. Electron*, 2020.

[14] P. Weetman and M. S. Wartak, "Wigner function modeling of quantum well semiconductor lasers using classical electromagnetic field coupling," *J. Appl. Phys.*, vol. 93, no. 12, pp. 9562–9575, 2003.